Bulletin of the Seismological Society of America, Vol. 86, No. 6, pp. 1845–1852, December 1996

Large-Amplitude Moho Reflections (*SmS*) from Landers Aftershocks, Southern California

by Jim Mori and Donald Helmberger

Abstract Closely spaced aftershocks of the 28 June 1992 Landers earthquake (M_w 7.3) were used to make event record sections that show the transverse components of *S* and *SmS* arrivals at a distance of 70 to 170 km. For the data recorded toward the north in the Mojave desert, large *SmS* phases are observed with amplitudes 2 to 5 times greater than the direct *S*. For similar distances to the south, the *SmS* arrival is comparable to or smaller than the *S*. Comparisons to synthetic seismograms indicate that the large-amplitude *SmS* phases are produced by the simple crustal structure of the Mojave desert that allows a large Moho reflection. In contrast, the more complex geologic structure to the south partitions the seismic energy into a more complicated set of seismic phases, so that the Moho reflection is diminished in amplitude. The large *SmS* phases observed in the Mojave enhance the overall ground motions by a factor of 2 to 3. This suggests that when damaging earthquakes occur in other regions of simple crustal structures, Moho reflections will produce amplified strong motions at distance ranges around 100 km depending on the local structure.

Introduction

In southern California, at epicentral distances of 80 to 120 km, one of the largest amplitude seismic arrivals can be the *S*-wave reflections (*SmS*) from the Mohorovicic discontinuity (Moho) between the crust and mantle. Because of its large amplitude, *SmS* can control the strong shaking from moderate and large earthquakes in this distance range. Using recorded strong-motion data from the 1968 Borrego Mountain earthquake, Burger *et al.* (1987) showed that the largest ground velocities at San Onofre were from *S* reflections off the Moho. Other observational studies (Somerville and Yoshimura, 1990; Somerville *et al.*, 1993) concluded that the strong shaking in San Francisco from the Loma Prieta earthquake was 2 or more times stronger because of the *SmS* phase. An understanding of *SmS* amplitudes is important for characterizing strong ground motions at distances around 100 km, and attenuation relations may be improved by accounting for the amplification (or lack of) caused by this phase.

This study uses closely spaced aftershock data from the 28 June 1992 Landers earthquake (M_w7.3) to make event record sections that show clear examples of the varying amplitudes of *SmS*. Some of the data show strong *SmS* phases that are 2 to 5 times larger than the direct *S* wave, while other recordings at comparable distances show *SmS* amplitudes that are smaller than the direct *S*. Using comparisons to synthetic seismograms, we explain the amplitude variations in terms of the local crustal and Moho structure. The results are used to infer general types of crustal structure that are likely to produce the large-amplitude *SmS* arrivals.

Data

This study takes advantage of the large amount of high-quality broadband data collected from the aftershocks of the Landers earthquake. By combining seismograms from closely spaced aftershocks recorded at single stations, detailed seismic sections can be constructed that show the complexity of the wave propagation with distance (i.e., Spudich and Bostwick, 1987; Mori, 1991). These resulting sections are similar to those produced by refraction experiments, except that refraction data usually have a few explosion sources with many recorders, while this study uses many sources recorded at a few stations. An important advantage of using earthquake sources is that one can see the waves that actually cause damage during an earthquake (i.e., *S*, *SmS*, and short-period surface waves). Experimental data using explosion sources contain less shear-wave energy, so these phases are commonly not well observed in refraction studies, and often it is necessary to use the strength of *PmP* to infer the behavior of the *S* reflections.

Figure 1 shows the locations of 107 Landers aftershocks ($M \geq 3.0$ to 4.0) and the two TERRAscope (Kanamori *et al.*, 1991) stations that recorded the data for this study. The aftershocks form a nearly linear array of sources that are recorded to the north at Goldstone (GSC) and to the south at Pinyon Flat (PFO). GSC is located nearly along strike of the Landers rupture, providing a simple geometry to form an event record section that extends for over 100 km. PFO toward the south is not aligned as closely to the strike di-

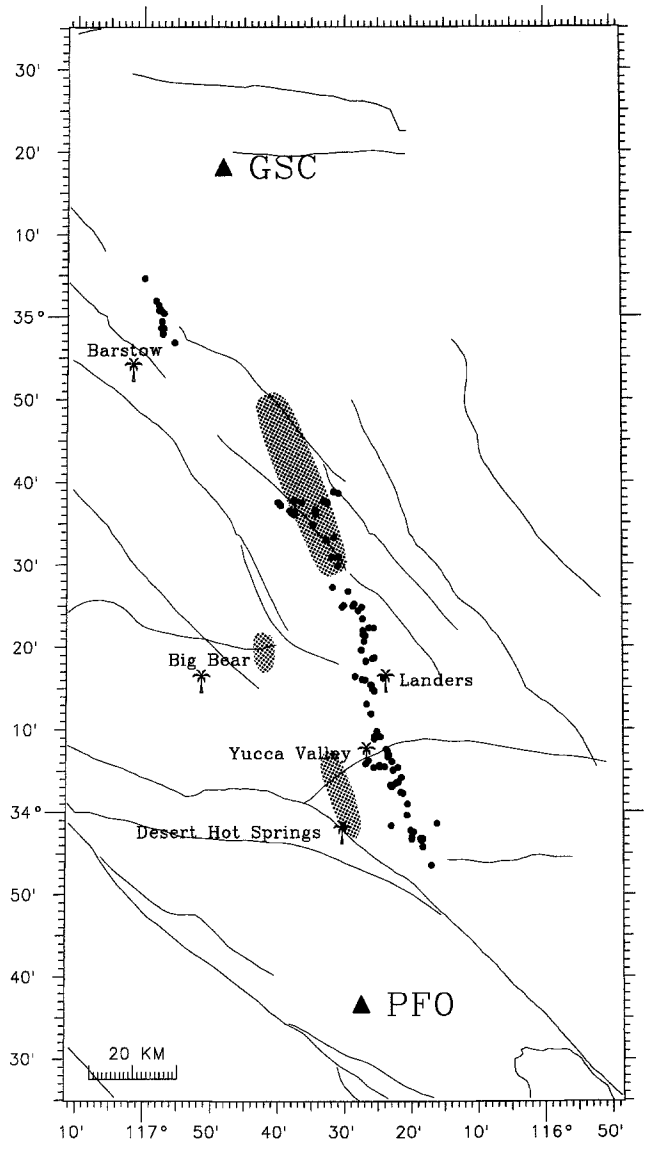

Figure 1. Locations of Landers aftershocks (filled circles) and TERRAscope stations (triangles) used in this study. Shaded regions show *SmS* bounce points, assuming the crustal structures in Tables 1 and 2.

rection, but the aftershocks still span a significant distance range to provide a good record section. Traces in the record sections were formed by rotating the two horizontal components of the velocity seismograms to the transverse direction and plotting them as a function of epicentral distance. All of the traces were lined up on the initial *P*-wave arrival, as timed from the vertical component. The traces are normalized by their peak amplitudes, since the absolute amplitudes vary considerably with the magnitudes of the earthquakes. The broadband TERRAscope data have a bandwidth of 0.0028 to 5 Hz, and the data of this study have energy predominantly in the range of 0.5 to 5 Hz. Since most of these events have strike-slip focal mechanisms (Hauksson *et al.*, 1993), using the transverse component has two advantages. First, the recording stations are nearly in the strike direction, so the transverse components have large, stable amplitudes. Second, the azimuthal effects of the radiation pattern are minimized, since the shape of transverse waveforms do not depend on azimuthal take-off angle for pure strike-slip mechanisms.

Figure 2 and 3 show the event record sections from GSC and PFO, respectively, for similar distance ranges of 70 to 170 km. Since the individual traces are normalized, these figures do not show the decay of absolute amplitudes with distance, but the data clearly show the relative amplitudes of the various phases in each seismogram. For the GSC data to the north of the aftershocks, the range of 80 to 120 km shows strong *SmS* arrivals 2 to 4 sec after the direct *S* with amplitudes that are several times larger than the direct *S*. The *SmS* energy is the largest feature on the GSC seismograms in this distance range. Using similar data at lower frequencies, Jones (1995) showed that the displacement seismograms from larger aftershocks at GSC also had large-amplitude *SmS* and *sSmS* arrivals. For the comparable distance range as recorded to the south at PFO, the *SmS* energy is not as apparent. In these data, the direct *S* arrivals are quite clear, and the following 5- to 8-sec windows have relatively large sustained amplitudes such that distinct *SmS* arrivals cannot be easily seen. The large gap in the record section between 115 and 160 km reflects the gap in the aftershocks seen in Figure 1. The GSC record section does not show this because the gap is at distances closer than 70 km.

In order to clarify the size of the *SmS* arrivals relative to the direct *S* in the GSC data, we produced a stacked record section in the distance range where the large Moho reflections are observed. The seismograms recorded from 75 to 110 km were rectified, and data within ranges of 10-km epicentral distances were averaged together (Fig. 4). All data from GSC and PFO were also processed in this same manner for comparisons with synthetic waveforms, which will be shown later. In this stacked record section, the direct *S* and *SmS* arrivals have about equal amplitudes from 75 to 85 km. At farther ranges of 90 to 110 km, which are past the critical distance, *SmS* amplitudes are observed to be much larger than the direct *S* by factors of 2 to 5.

S and *SmS* Amplitudes versus Distance

The GSC record section (Fig. 2) and the stacked version (Fig. 4), which are both trace normalized, clearly show *SmS* amplitudes that are significantly larger (2 to 5 times the amplitude) than the direct *S*. One important distinction to be made is whether the amplitude of the direct *S* is unusually small or the amplitude of the *SmS* is unusually large. If the *S* waves are small, the *SmS* amplitudes may be large only relative to the direct *S* and would not be indictative of enhanced ground shaking. If we examine the coda levels in Figure 2, we can see that there is a distinct reduction in coda amplitudes for those events at distances around 90 km. This is not observed in Figure 3, which suggests that *SmS* arrivals

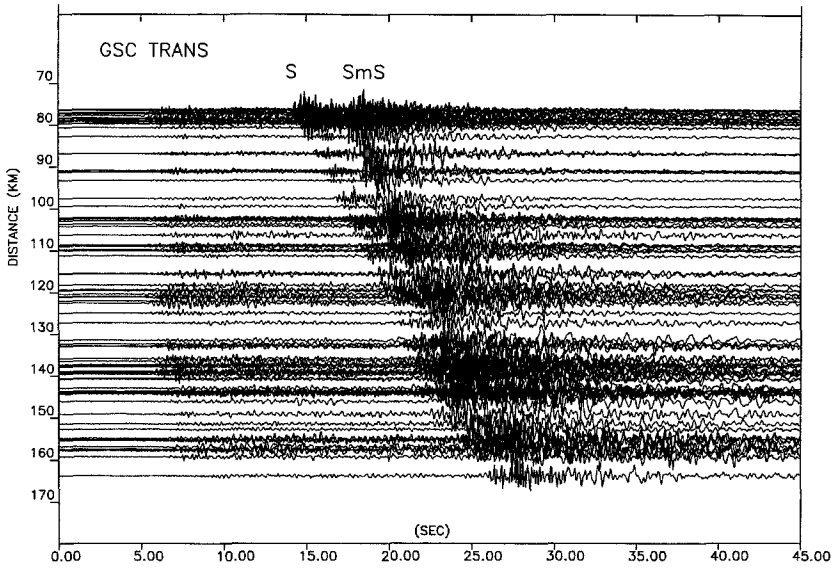

Figure 2. Event record section composed of the transverse components of velocity from Landers aftershocks recorded toward the north in the Mojave desert at GSC. Note the large *SmS* arrivals several seconds after the *S* in the distance range of 80 to 120 km.

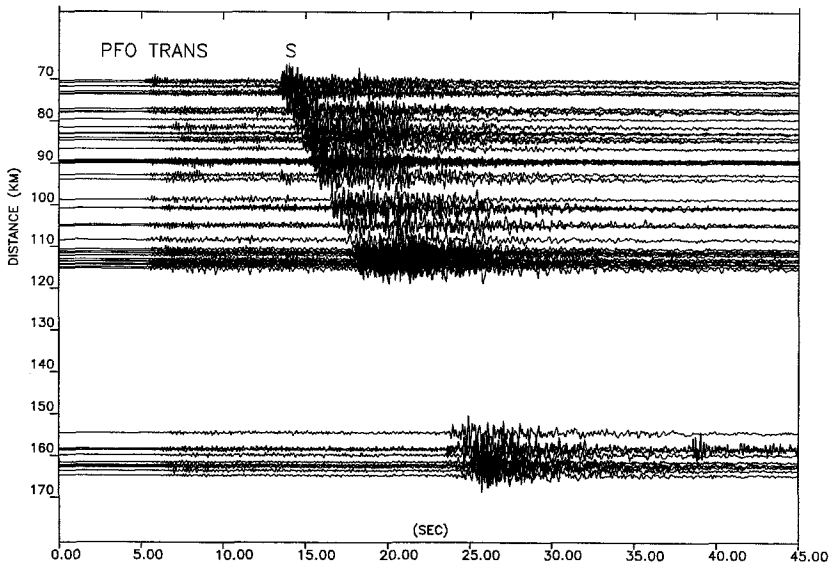

Figure 3. Event record section composed of the transverse components of velocity from Landers aftershocks recorded toward the south at PFO.

do have larger absolute amplitudes in the GSC profile. To investigate this issue, we measured the peak velocity amplitudes of the transverse components and normalized them by the anti-log of the earthquake magnitude (Fig. 5). The magnitudes were taken from the Southern California Seismic Network catalog, which are typically determined using 20 to 30 amplitude readings in the 1- to 5-Hz range from stations distributed throughout southern California (Wald *et al.*, 1995).

Figure 5 shows the distance dependence of the amplitudes as recorded at the two sites. For the PFO data recorded to the south of the aftershocks, the amplitude data show a smooth decay as a function of distance, which is typical of the *S* wave at these distances. There is a relatively large amount of scatter in the amplitude data, which may be attributed to differences in source depth and focal mechanism. In contrast to the PFO data, the GSC amplitudes are 2 to 3 times larger than the general trend at distances of 80 to 105 km, which is the range where the large *SmS* arrivals are observed in the record sections of Figures 2 and 4. These results show that the *SmS* arrivals produce real enhanced amplitudes. However, the amplitudes are larger by only a factor of 2 to 3, not the full value of the *SmS* to direct *S* amplitude ratio. Comparison to the synthetic seismograms later in this article will show that the large ratio of *SmS* to direct *S* amplitudes is due to both large *SmS* arrivals and small direct *S* arrivals.

Comparison to Model Synthetics

The striking difference in the *SmS* amplitudes recorded to the north at GSC and to the south at PFO can be attributed to the differences in the local crustal and Moho structures. It is not a source effect since the same set of earthquakes are

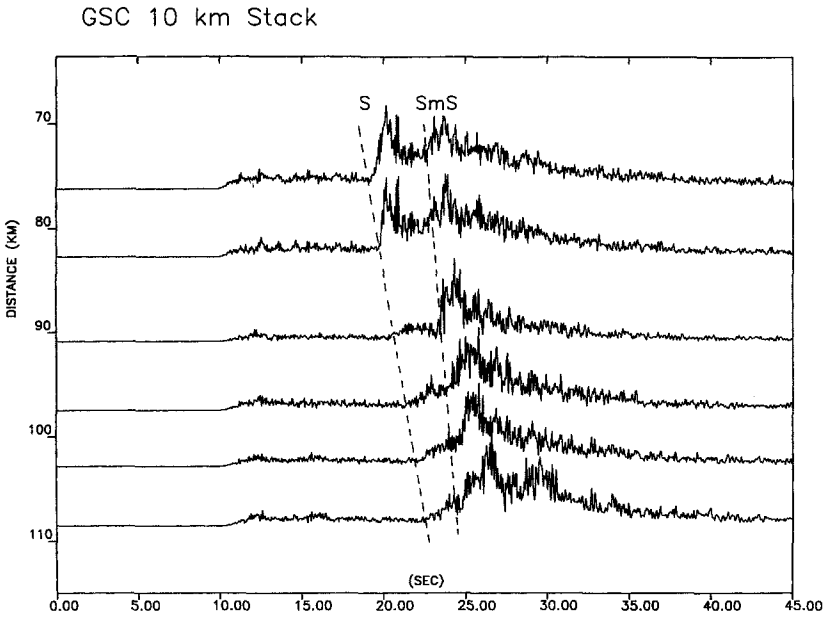

Figure 4. Rectified and stacked record section of part of the GSC profile showing the large amplitude of *SmS* compared to the *S* wave.

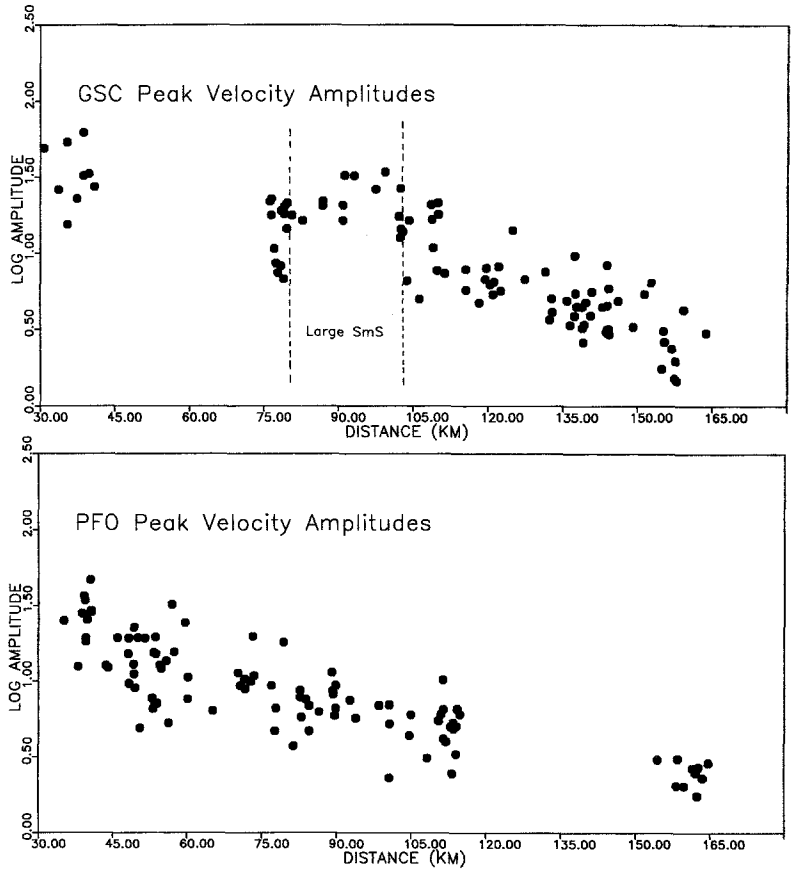

Figure 5. Maximum velocity amplitudes of the Landers aftershocks, normalized by magnitude, for the transverse component of velocity. Top shows amplitudes recorded toward the north in the Mojave desert at GSC, and bottom shows amplitudes toward the south at PFO. Dotted lines in the GSC data show the distance range where the large *SmS* arrivals are observed.

used for both record sections. Also, it is not due to the radiation pattern, since the transverse components from strike-slip mechanisms have weak azimuthal dependence. To show the effect of the local crustal and Moho structure, we calculated generalized ray synthetic seismograms (Helmberger, 1983) for two simple models. The point of the synthetic calculations was not to match all the various crustal arrivals, but rather to understand the general characteristics of the amplitudes and waveform. No attempt was made to adjust the velocity models to match the data; instead, velocity models derived from previous studies were used to try and understand the variations in the *S* and *SmS* amplitudes. The

source for all the synthetics was a vertical strike-slip fault at 10 km depth with a short duration of 0.2 sec.

For the Mojave desert, model 1 (Table 1) is a simple *S*-wave model that consists of a one-layer crust, overlain by two shallow layers and a Moho at 28 km. Below the Moho, there is a mantle velocity of 4.3 km/sec. This structure has been used by Jones (1995) in studies to model propagation paths across the Mojave desert and seems appropriate for paths from the Landers aftershocks northward toward GSC. The synthetic seismograms for this Mojave structure (Fig. 6) show large *SmS* phases throughout the distance range and a relatively small direct *S* arrival. The *sS* has even smaller amplitudes than the direct *S* and essentially cannot be seen in the synthetics. The Moho reflection is largest past the critical distance (68 km for a 10-deep source) where the reflection coefficient from the Moho is 1.0. Both the direct *S* and the *SmS* phases diminish in amplitude with distance because of geometric spreading and changes in the transmission coefficient of the shallower layers. This general pattern of roughly equal *S* and *SmS* at closer distances (70 to 80 km) and then much larger *SmS* at greater distances (>80 km) can be seen on the data recorded at GSC (Figs. 2 and 4).

The second velocity structure, which is more appropriate to regions of southern California west of the San Andreas fault (Helmberger *et al.*, 1993), is slightly more complicated with two crustal layers overlain by the same two shallow layers used in the Mojave model. The thicknesses and velocities of the crustal layers were originally determined from blast data by Hadley and Kanamori (1979). The Moho is at a 35-km depth with a mantle velocity of 4.4 km/sec (Table 2). Because of the additional "Conrad discontinuity," the synthetic seismograms become more complicated as the crustal layering produces more arrivals (Fig. 7). There is a recognizable *SmS* that has largest amplitudes near the critical distance of 105 km, but compared to the Mojave structure, it is weaker and mixed with other crustal phases. The overall effect of adding the extra crustal layer of the southern California model is to produce more complexity in both the *S* and *SmS*. For the *S* wave, the interactions with the crustal layering produces a packet of several arrivals that always has fairly large amplitudes throughout the record section. The interactions of *SmS* as it passes through the crustal layers tend to reduce its amplitude. Compared to the Mojave structure, the *SmS* is not seen as distinctly because of the larger-amplitude *S*-wave packet, the smaller-amplitude *SmS*, and the various complicating phases. These effects in obscuring the *SmS* arrivals are amplified in the data where the arrivals are not simple pulses but high-frequency envelopes with a duration of several seconds (Fig. 3).

In order to make a better comparison between the model calculations and show that the propagation effects described above are consistent with the observed data, we convolved a "source envelope" with the point source synthetics. The point source synthetics are similar to those shown in Figures 6 and 7, but without a 0.2-sec source duration. The source envelope was derived by averaging together traces of data from both GSC and PFO and contains an estimate of the high-frequency duration of the *S*- or *SmS*-wave packet seen in the data. In order to minimize the effects of multiple phases in the source envelope, we chose data in which a single arrival

Table 1
Mojave Velocity Structure with a Moho at 28 km Depth

Depth (km)	*S* Velocity (km/sec)
0.0	2.6
2.5	3.5
5.5	3.6
28.0	4.3

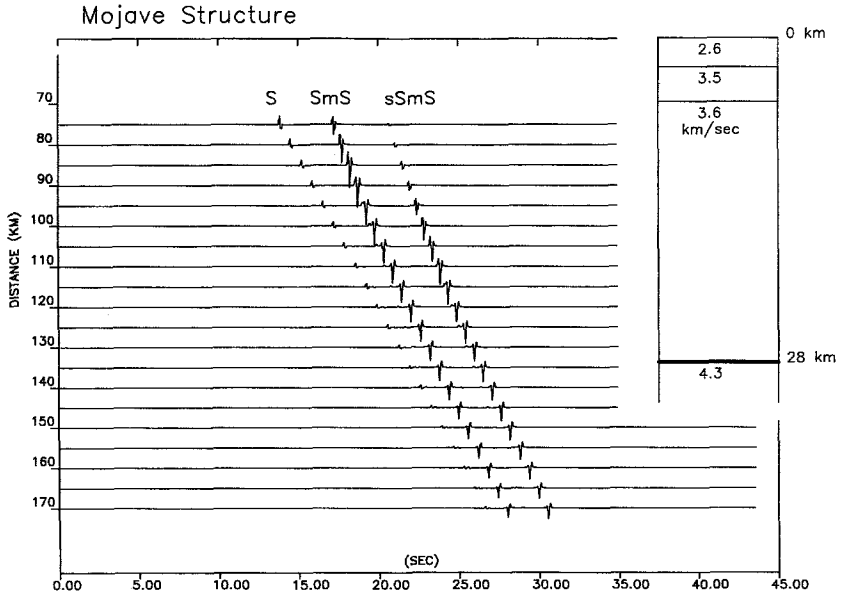

Figure 6. Synthetic seismograms for the Mojave velocity structure (Table 1). The source is a vertical strike-slip fault at 10 km depth.

predominated. We used data from the *SmS* arrival at GSC in the distance range of 85 to 105 km and data for the direct-*S* at PFO in the range of 75 to 90 km. The same source envelope was used in both the GSC and PFO comparisons (Fig. 8). After convolving with the source envelope, the synthetics were rectified and stacked in the same manner as the data. The synthetic seismograms from the Mojave velocity structure are shown with the GSC profile in Figure 8, and the synthetics for the southern California model are shown with the PFO data in Figure 9. The data in these two figures are the record sections rectified and stacked as described previously in the data section.

It is difficult to model all the high-frequency characteristics of the recorded data, but examination of the stacked waveforms show correlated features that can be simulated. In particular, we can investigate the relative arrival times and amplitudes between *S* and *SmS*. The stacking procedure will tend to minimize variations in focal mechanisms and directivity effects that can affect the amplitudes. For the GSC comparison, both the data and the synthetics show equal amplitude wave packets for the *S* and *SmS* at closer ranges (75 to 85 km), then much smaller-amplitude *S* waves at distances greater than 85 km. The PFO data and synthetics have a different character, with a large *S*-wave packet (consisting of direct *S* and secondary arrivals generated by the velocity contrast at 16 km depth) throughout the record section followed by a series of other arrivals that includes the *SmS*. Another difference between the two record sections is that the largest amplitudes of *SmS* (indicating the distance near the critical reflection) are near 80 km for the GSC profile and near 105 km for the PFO profile. This difference in the critical distance is a due to the regional differences in Moho depth (assuming flat-lying structures) and the crustal structure.

Both synthetic record sections show large-amplitude surface reflections (*sS* and *sSmS*) that are not clearly seen in the data. The lack of large free-surface phases may be due to radiation patterns that are different from the assumed vertical strike-slip mechanisms, or due to near-surface material that would tend to scatter and attenuate these phases at high frequency. The conjecture that shallow structure may be scattering and attenuating these high-frequency arrivals is supported by the observations that surface reflections are more easily observed in broadband data (Helmberger *et al.*, 1993; Jones, 1995), where the longer periods are not as sensitive to the shallow structure. Also, all the aftershocks are not at the same 10-km source depth assumed in the synthetics, so that there would be much less coherence of the free-surface reflections in the event record section that combines all these events.

Table 2
Southern California Velocity Model with a Moho at 35 km Depth

Depth (km)	*S* Velocity (km/sec)
0.0	2.6
2.5	3.5
5.5	3.6
16.0	3.9
35.0	4.4

Discussion

Synthetic seismograms calculations (Burger *et al.*, 1987; Helmberger *et al.*, 1993) and strong-motion observations from Loma Prieta (Somerville *et al.*, 1993; McGarr *et al.*, 1991) indicate that Moho reflections can control the amplitudes at distances near 100 km. However, amplifying effects from *SmS* can vary significantly. In this study, we report on large *SmS* amplitudes observed in the Mojave desert that increase the ground motions by a factor of 2 to 3, compared with smaller *SmS* arrivals in the opposite direction that

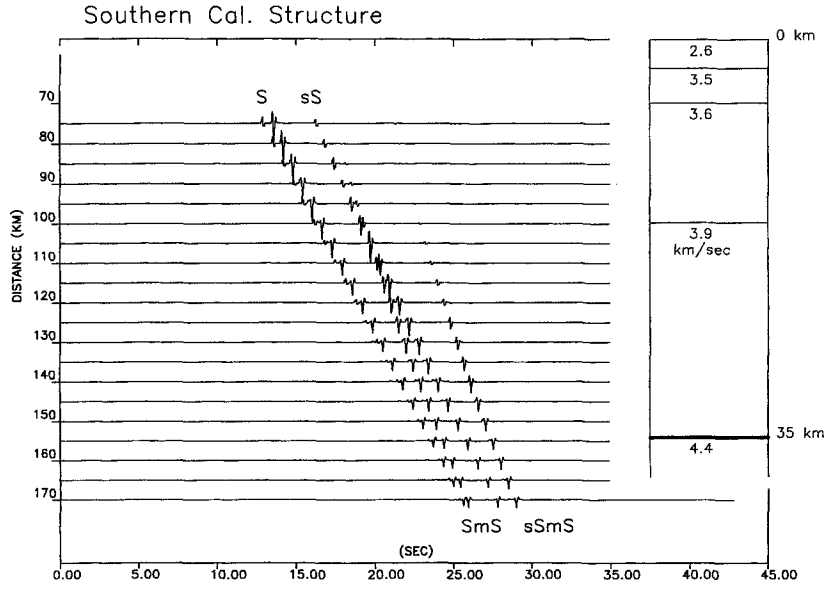

Figure 7. Synthetic seismograms for the southern California velocity structure (Table 2). The source is a vertical strike-slip fault at 10 km depth.

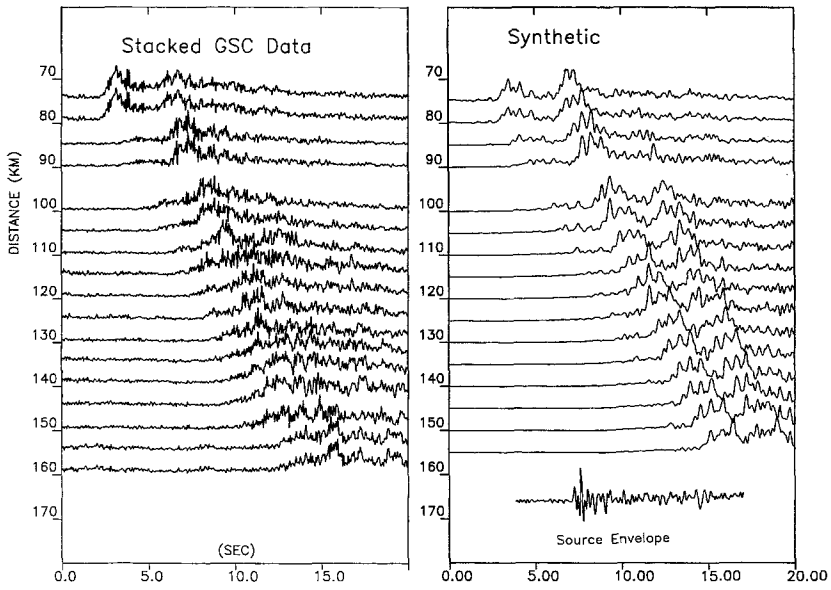

Figure 8. Comparison of rectified and stacked data from GSC with synthetic seismograms calculated using the Mojave velocity structure. The synthetics include a convolution with the source envelope shown in the bottom right.

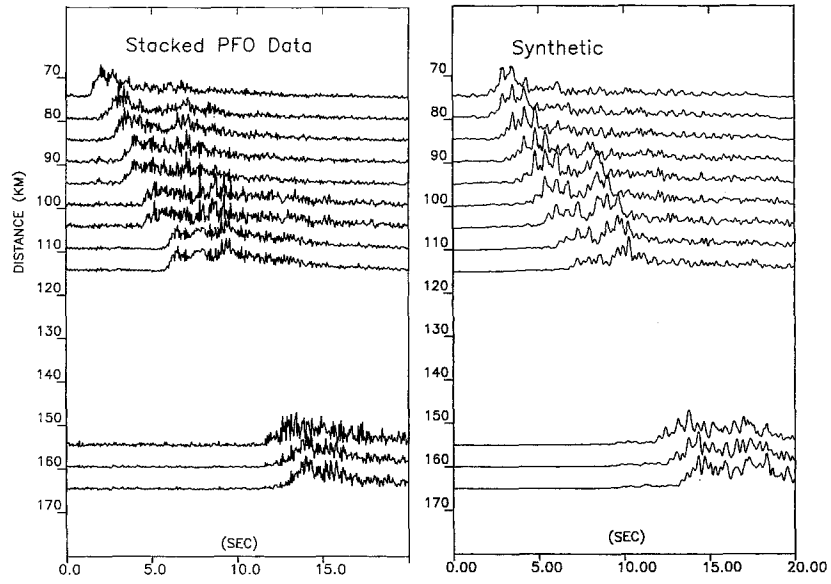

Figure 9. Comparison of rectified and stacked data from PFO with synthetic seismograms calculated using the southern California velocity structure. The synthetics include a convolution with the source envelope shown in Figure 8.

do not amplify the overall motions. Statistical studies of earthquake magnitude determinations show systematically large amplitudes at distance ranges of 75 to 125 km for central California (Bakun and Joyner, 1984) and around 60 km for southern California (Hutton and Boore, 1987). These enhanced amplitudes might be attributed to *SmS* arrivals; however, in these studies, which include thousands of amplitudes, there is an average increase of only about 25%. The large amplifications observed in individual studies and the rather small average increase in the statistical studies suggest that there are limited conditions where the *SmS* causes the large-amplitude enhancements.

The results of this study indicate that the regions of simple crustal structure can produce the large-amplitude *SmS* arrivals. Simple crustal structures, such as observed in the Mojave desert north of the Landers aftershocks, allow a large reflection from the Moho since there is little interaction of the phase with other crustal features. The results seen in the synthetic seismogram profiles show that the addition of just one more layer, such as the Conrad discontinuity, can significantly reduce the size of this reflection. As the velocity structure becomes more complex, the energy tends to be partitioned into more phases, so the amplitude of any one phase such as *SmS* tends to become smaller. The smaller *SmS* amplitudes observed at PFO along a path of more complicated geologic structures are consistent with this result. The actual velocity structure from the Landers aftershocks to PFO is probably even more complicated than the southern California model used in this study. There could be two- and three-dimensional effects since the ray paths cross the San Andreas fault and Transverse Ranges. All of these added structures would tend to further reduce the size of the Moho reflection, so it is not surprising that the *SmS* amplitudes are not very large. This conclusion about simple crustal struc-

tures is also consistent with the results of Burger *et al.*, where they used a homogeneous crustal structure to model the large *SmS* phases observed from the Borrego Mountain earthquake.

An alternative explanation of the difference in *SmS* amplitudes at GSC and PFO is that there is a regional southward dip to the Moho, which would be consistent with the different Moho depths in the two models used in this study, and also the results of Hearn (1984). Such a dipping Moho would tend to produce larger-amplitude reflection in the updip direction toward GSC, compared to the downdip direction toward PFO. This effect is seen in data from an active seismic experiment in the region of the 1989 Loma Prieta earthquake, where large-amplitude reflections are attributed to a dipping Moho (Catchings and Kohler, 1996). This interpretation accounts for the difference in *SmS* amplitudes but does not explain the greater complexity in the waveforms that are observed in the data recorded at PFO. Moho dip may be a factor in producing the difference in *SmS* amplitudes, but more complex structure toward the south is still necessary to produce the more complicated waveforms.

The large scatter in amplitude data due to regional crustal structure is not limited to the *SmS* arrivals. Regressions of amplitudes from strong-motion data, which are comprised of primarily *S* waves, also have large variability that can be attributed to local crustal and site structures (i.e., Joyner and Boore, 1981). However, understanding the amplitude effects of the *SmS* phase and other lower crustal arrivals can lead to better regional estimates of the strong motions produced by damaging earthquakes at distances near 100 km.

Conclusions

We have shown that for seismograms recorded to the north of the Landers aftershocks in the Mojave desert, there are large-amplitude *SmS* phases that amplify the peak ground motions by factors of 2 to 3. From comparisons of the data with synthetic seismograms, we can attribute the large-amplitude *SmS* phases to simple crustal structure that allows simple reflections from the Moho. This is in contrast to the region south of the Landers aftershocks where more complicated crustal structure produces less distinctive Moho reflections. Extending this interpretation to other regions, we infer that in areas with simple flat-lying crustal structures, especially where there is no Conrad discontinuity, one would expect Moho reflections to produce amplified ground motions in the distance range around 100 km.

Acknowledgments

We thank H. Benz, G. Fuis, R. Herrmann, and P. Somerville for useful comments on this article. Waveform data were retrieved from the Southern California Earthquake Center Data Center. Partial funding for this project was provided by the Nuclear Regulatory Commission and by the U.S. Geological Survey, Grant 1434-93-G-2322. Contribution 5570, Division of Geological and Planetary Sciences, California Institute of Technology.

References

Bakun, W. H. and W. B. Joyner (1984). The M_L scale in central California, *Bull. Seism. Soc. Am.* **74,** 1827–1843.

Burger, R. W., P. G. Somerville, J. S. Barker, R. B. Herrmann, and D. V. Helmberger (1987). The effect of crustal structure on strong ground motion attenuation relations in eastern North America, *Bull. Seism. Soc. Am.* **77,** 420–439.

Catchings, R. D. and W. M. Kohler (1996). Reflected seismic waves and their effect on strong shaking during the 1989 Loma Prieta, California, earthquake, *Bull. Seism. Soc. Am.* **86,** 1401–1416.

Hadley, D. and K. Kanamori (1979). Regional S-wave structure for southern California from analysis of teleseismic Rayleigh waves, *Geophys. J. R. Astr. Soc.* **58,** 655–666.

Hauksson, E., L. M. Jones, K. Hutton, and D. Eberhart-Phillips (1993). The 1992 Landers earthquake sequence: seismological observations, *J. Geophys. Res.* **98,** 19835–19858.

Hearn, T. M. (1984). Pn travel times in southern California, *J. Geophys. Res.* **89,** 1843–1855.

Helmberger, D. V. (1983). Theory and application of synthetic seismograms, in *Earthquakes: Observation, Theory and Interpretation, Proc. Int. Sch. Phys. 'Enrico Fermi' course LXXXV,* H. Kanamori and E. Boschi (Editors), North-Holland, Amerdam, 174–221.

Helmberger, D., D. Dreger, R. Stead, and H. Kanamori (1993). Impact of broadband seismology on the understanding of strong motions, *Bull. Seism. Soc. Am.* **83,** 830–850.

Hutton, L. K. and D. M. Boore (1987). The M_L scale in southern California, *Bull. Seism. Soc. Am.* **77,** 2074–2094.

Jones, L. (1995). Part I: Broadband modeling of aftershocks from the Joshua Tree, Landers, and Big Bear sequences, southern California, *Thesis,* California Inst. Tech., 180 pp.

Joyner, W. B. and D. M. Boore (1981). Peak horizontal acceleration and velocity from strong-motion records, including records from the 1979 Imperial Valley, California, earthquake, *Bull. Seism. Soc. Am.* **71,** 2011–2038.

Kanamori, H., E. Hauksson, and T. Heaton (1991). TERRAscope and CUBE project at Caltech, *EOS* **72,** 564.

McGarr, A., M. Celebi, E. Sembara, T. Noce, and C. Mueller (1991). Ground motion at the San Francisco International Airport from the Loma Prieta earthquake sequence, 1989, *Bull. Seism. Soc. Am.* **81,** 1923–1944.

Mori, J. (1991). Estimates of velocity structure and source depth using multiple P waves from aftershocks of the 1987 Elmore Ranch and Superstition Hills, California, earthquakes, *Bull. Seism. Soc. Am.* **81,** 508–523.

Somerville, P. and J. Yoshimura (1990). The influence of critical Moho reflections on strong ground motions recorded in San Francisco and Oakland during the 1989 Loma Prieta earthquake, *Geophys. Res. Lett.* **17,** 1203–1206.

Somerville, P. G., N. F. Smith, and R. W. Graves (1993). Effect of critical reflections from the Moho on the attenuation of strong ground motion, in *The Loma Prieta, California Earthquake of October 17, 1989—Strong Ground Motion, U.S., R. D. Borcherdt (Editor), Geol. Surv. Profess. Pap. 1551-A,* 67–76.

Spudich, P. and T. Bostwick (1987). Studies of the seismic coda using earthquake cluster as a deeply buried seismograph array, *J. Geophys. Res.* **92,** 10526–10546.

Wald, L. A., L. K. Hutton, and D. D. Given (1995). The southern California network bulletin: 1990–1993 summary, *Seism. Res. Lett.* **66,** 9–19.

U.S. Geological Survey
525 South Wilson Ave.
Pasadena, California 91106
(J.M.)

California Institute of Technology
Pasadena, California 91125
(D.H.)

Manuscript received 12 September 1995.